

LETTER • OPEN ACCESS

Spatial polarization variation in terahertz electromagnetic wave focused by off-axis parabolic mirror

To cite this article: Mayuko Takai *et al* 2016 *Appl. Phys. Express* **9** 052206

View the [article online](#) for updates and enhancements.

You may also like

- [Ultrametric identities in glassy models of natural evolution](#)
Elena Agliari, Francesco Alemanno, Miriam Aquaro *et al.*
- [A 20-channel magnetoencephalography system based on optically pumped magnetometers](#)
Amir Borna, Tony R Carter, Josh D Goldberg *et al.*
- [High-sensitivity operation of single-beam optically pumped magnetometer in a kHz frequency range](#)
I Savukov, Y J Kim, V Shah *et al.*

Spatial polarization variation in terahertz electromagnetic wave focused by off-axis parabolic mirror

Mayuko Takai¹, Kazunori Shibata², Mitsuharu Uemoto³, and Shinichi Watanabe^{1*}

¹Department of Physics, Faculty of Science and Technology, Keio University, Yokohama 223-8522, Japan

²RIKEN SPring-8 Center, Theory Team, Sayo, Hyogo 679-5148, Japan

³Center for Computational Sciences, University of Tsukuba, Tsukuba, Ibaraki 305-8577, Japan

*E-mail: watanabe@phys.keio.ac.jp

Received February 24, 2016; accepted March 28, 2016; published online April 13, 2016

We have investigated the spatial distribution of the polarization state of a terahertz electromagnetic wave focused by an off-axis parabolic mirror (OPM) in the focal plane. We employed polarization-resolved terahertz time-domain spectroscopy and found that a steep spatial variation in the polarization state appears slightly distant from the focus when a linearly polarized terahertz wave is focused. The spatial variation includes an abrupt change in the polarization state (states change between circular and linear polarizations) within a wavelength. The observed phenomena are confirmed by numerical calculations and are shown to be intrinsic to the reflection from the OPM.

© 2016 The Japan Society of Applied Physics

An intense and single-cycle terahertz electric field (E-field) can dramatically change or coherently control the electronic and magnetic properties of materials; this phenomenon has been the subject of extensive research in the optics and photonics communities for decades. There are many reports on various nonlinear optical processes in ferroelectric materials,^{1,2)} semiconductors,^{3–10)} metals,¹¹⁾ and superconductors¹²⁾ due to the intense terahertz pulse irradiation. In addition, control of the spin dynamics through a direct interaction between the spins and magnetic field components of the intense terahertz pulse^{13–17)} and through an electric-dipole active spin excitation in multiferroics has been achieved.¹⁸⁾ The analysis of the spin precession dynamics can be described by solving the Landau–Lifshitz–Gilbert equation,^{14,18)} including the temporal variation in the terahertz electromagnetic vector. A precise knowledge of the polarization states of the applied terahertz pulse, i.e., a time evolution of the E-field vector focused on the sample, is thus required. Knowledge of the polarization states is also required for performing ellipsometry with polarization-resolved terahertz time-domain spectroscopy systems,^{19–22)} as well as for terahertz polarization imaging applications.^{23–25)}

An off-axis parabolic mirror (OPM) is often used in the foregoing experiments. The OPM is useful for collecting every frequency component of the terahertz pulse in the unique focus because of the absence of chromatic aberration. As a result, a single-cycle terahertz pulse with a large E-field amplitude, exceeding 1 MV/cm, has been realized by a tabletop regenerative amplifier system.²⁶⁾ The spatial resolution of terahertz time-domain spectroscopy is also increased with the use of an OPM with a large numerical aperture. However, there have been few studies on the polarization properties of a focused terahertz pulse using the OPM. Polarization rotation of the focused terahertz pulse has been occasionally observed,²²⁾ but it has been considered to originate owing to the misalignment of the OPM. Recently, we reported the observation of the intrinsic polarization modulation of a terahertz electromagnetic wave focused by the OPM.²⁷⁾ In this paper, the discussion concentrated on the area near the focus, and the amount of the polarization modulation was not so large in this area.

In this letter, we report on the polarization state variation in the terahertz wave focused by the OPM in a wider area of

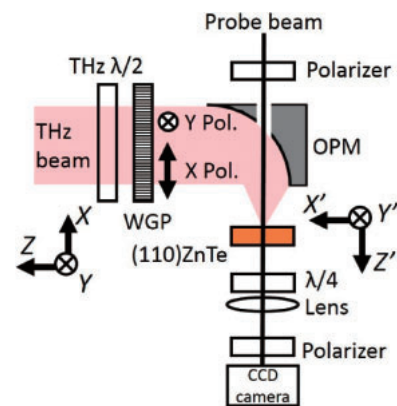


Fig. 1. Schematic of the experimental setup. The terahertz pulse arrives from the left-hand side of the figure. THz $\lambda/2$: half-wave plate for the wavelength of 496 μm ; WGP: wire-grid polarizer; OPM: off-axis parabolic mirror with a diameter of 50.8 mm and effective focal length of 50.8 mm; $\lambda/4$: quarter-wave plate optimized at the wavelength of the near-infrared range; Lens: biconvex lens (focal length = 50 mm); and polarizer: a Glan–Thompson prism. The XYZ and $X'Y'Z'$ systems are shown.

the focal plane. When a linearly polarized terahertz wave is focused, the polarization state substantially deviates from its original state at positions slightly distant from the focus. In particular, a steep spatial variation in the polarization state is observed on a line perpendicular to the symmetric axis of the OPM, traversing the focus; the polarization state changes abruptly between circular and linear polarizations within a single wavelength. We confirmed the result by numerical calculations; the observed result is not caused by misalignment of the OPM, but it is due to the phenomenon being intrinsic to the reflection from the OPM.

Figure 1 shows a schematic of the experimental setup. We used a titanium-sapphire regenerative amplified laser system (Clark-MXR CPA-2010) as the light source to generate and detect terahertz pulses using the conventional terahertz time-domain spectroscopy setup. For terahertz pulse generation, we used optical rectification in a LiNbO_3 crystal through the tilted-pump-pulse-front method.²⁸⁾ The emitted terahertz pulse is collimated using two OPMs (not shown in Fig. 1). Then it passes through a half-wave plate for the wavelength of 496 μm and a wire-grid polarizer to realize a terahertz pulse linearly polarized along either the Y - or X -axis. The

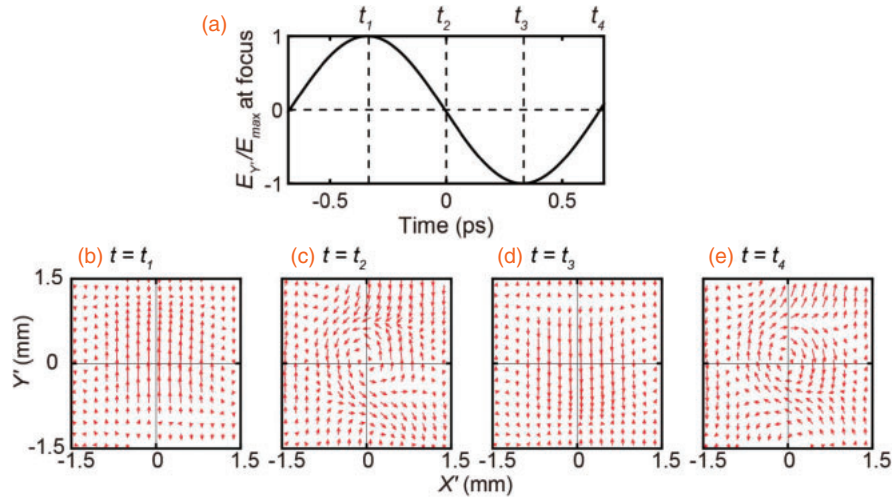


Fig. 2. (a) Time-domain waveform of the 0.75 THz frequency component of the terahertz pulse at the focus. We plot the Y' component. (b)–(e): Spatial mappings of the terahertz E-field vector in the focal plane at four different times: (b) $t_1 = -0.33$ ps, (c) $t_2 = 0$ ps, (d) $t_3 = 0.33$ ps, and (e) $t_4 = 0.67$ ps. For clarity, the lengths of the arrows in (b) and (d) are reduced by a factor of $2/5$ as compared to (c) and (e).

pulse is then focused onto a $\langle 110 \rangle$ -oriented zinc-telluride (ZnTe) crystal by an OPM with an effective focal length of 50.8 mm and a diameter of 50.8 mm. The thickness of the ZnTe crystal is 1 mm. The symmetric axis of the OPM, i.e., the symmetric axis of the paraboloid of which the OPM forms part, is parallel to the X' -axes.

The spatial mapping of the focused terahertz E-field vector on the crystal is realized by the spinning electro-optic sensor method combined with a charge-coupled device (CCD)^{29,30} as follows. We illuminated a probe pulse onto the ZnTe crystal, which quickly rotated with a frequency of 94.7 Hz. The diameter of the probe pulse is approximately 5 mm. Polarization rotation of the probe pulse is induced by the Pockels effect, which is caused by the terahertz E-field in the ZnTe crystal. After passing through the ZnTe crystal, the probe pulse passes through a quarter-wave plate and a Glan–Thompson prism, and the amount of the polarization rotation was monitored by the CCD. We analyzed the dependence of the Pockels effect on the ZnTe crystal angle to retrieve the E-field vector information. The time-domain information was obtained by moving an optical delay line every $2 \mu\text{m}$, which corresponds to 13.3 fs time intervals, and the E-field vector images were measured at 301 points. At each pixel, we performed the Fourier transform on the X' and Y' components of these 301 time-domain images into the frequency domain and obtained the amplitude and phase. The measured terahertz pulse ranges from approximately 0.25 to 1.0 THz. For a specific frequency component, the time-domain E-field vector spatial distribution is obtained by the inverse Fourier transform. The spatial resolution of the system is determined by the pixel size of the CCD, which is $62.5 \mu\text{m}$.

Figure 2(a) shows the time-domain waveform of the 0.75 THz frequency component of the terahertz E-field at the focus. The incident terahertz wave is linearly polarized along the Y -axis. We plot the Y' component in Fig. 2(a), where the Y' -axis is parallel to the Y -axis (see Fig. 1). We define the focus by the position where the Y' component has the maximum value. We define four characteristic times in the time-domain waveform. The Y' component $E_{Y'}$ takes the maximum value at $t = t_1$, minimum value at $t = t_3$, and zero at $t = t_2$ and t_4 . Thus, t_2 , t_3 , and t_4 are defined as the times

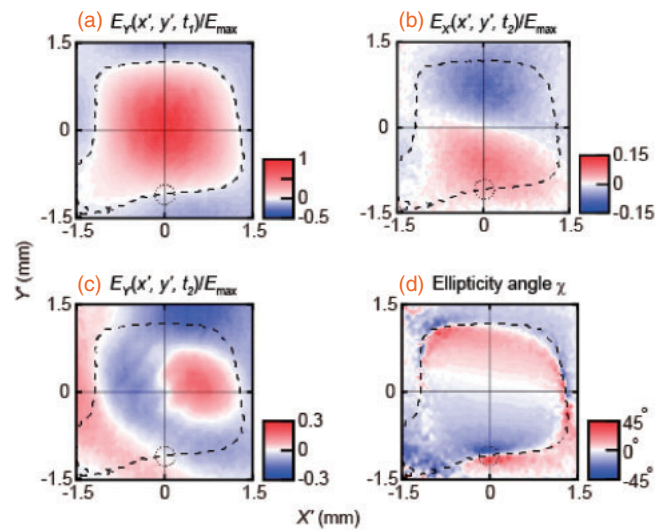


Fig. 3. Contour maps of experimental results of (a) $E_{Y'}(x', y', t_1)$, (b) $E_{X'}(x', y', t_2)$, (c) $E_{Y'}(x', y', t_2)$ normalized by E_{max} , and (d) ellipticity angle χ . The dashed curve in each image represents $E_{Y'}(x', y', t_1) = 0$. The black dotted circles indicate the position of $E_{Y'}(x', y', t_1) = 0$ on the Y' -axis, which is explained in the text.

that are $1/4$, $1/2$, and $3/4$ periods after t_1 , respectively. Figures 2(b)–2(e) show the spatial mappings of the terahertz E-field vector in the focal plane at the four characteristic times. At $t = t_1$ and t_3 , all the E-field vectors point in the positive or negative Y' -direction. On the other hand, at $t = t_2$ and t_4 , the E-field vector distributions show rotating structures in the counterclockwise or clockwise direction at the vicinity of the focus, respectively.²⁷⁾ The rotational vector distributions collapse at positions where the distance from the focus is longer than the wavelength (0.4 mm).

Next, we discuss the polarization state at each position in the focal plane. Figures 3(a)–3(c) show the spatial distributions of $E_{Y'}(x', y', t_1)$, $E_{X'}(x', y', t_2)$, and $E_{Y'}(x', y', t_2)$, respectively, for 0.75 THz. $E_{X'}(x', y', t_1)$ is almost zero in the entire focal plane. Note that we always consider the polarization state at each position in the focal plane, and the third argument always represents time. The E-field vector is normalized by $E_{\text{max}} = E_{Y'}(0, 0, t_1)$. In Fig. 3(a), we observed

a rectangular beam profile, which may be explained by the Fraunhofer diffraction pattern that is realized by the OPM with a rectangular aperture, because the shape of the half-wave plate is rectangular, and its size ($20 \times 20 \text{ mm}^2$) is smaller than the size of the OPM. The beam profile is not perfectly rectangular in the area where $x', y' < 0$; it is partly reproduced by the numerical calculation as shown later. This might be due to the asymmetric shape of the OPM as well as the misalignment of the measurement system. In Figs. 3(b) and 3(c), we observed a nonzero E-field in the focal plane, although it is almost zero at the focus. In Fig. 3(b), the E-field is almost zero along the X' -axis. On this axis, the terahertz wave is linearly polarized along the Y' -axis, which is the same as the initial polarization state before it is focused by the OPM. However, $E_{X'}(x', y', t_2) = 0$ is not satisfied at most positions in the focal plane. At these positions, the terahertz wave is not linearly polarized in the Y' -direction, but the E-field oscillating in the X' -direction mixes with that oscillating in the Y' -direction with a different phase. Therefore, the polarization state strongly depends on the position in the focal plane; the polarization is elliptical at some positions.

More quantitatively, we discuss the ellipticity angle χ ($-45^\circ \leq \chi \leq 45^\circ$) at each position in the focal plane, where linear and circular polarizations correspond to $\chi = 0^\circ$ and $\pm 45^\circ$, respectively, with the sign indicating the sense of rotation. Figure 3(d) shows a contour plot image of the spatial variation in χ . It is remarkable that the linear polarization expressed by $\chi = 0^\circ$ is realized only along the X' -axis and around the indicated curve of $E_{Y'}(x', y', t_1) = 0$. Even at positions where $\chi = 0^\circ$ holds, the terahertz wave is not necessarily polarized along the Y' -axis. For example, it is linearly polarized almost along the X' -axis at the position indicated by the dotted circle in Fig. 3, where $E_{Y'}(x', y', t)$ is always close to zero. Furthermore, there exist positions where χ is almost $\pm 45^\circ$, i.e.; the terahertz wave is almost circularly polarized. Note that such points are very close to the positions where $\chi = 0^\circ$ holds. Therefore, linear and circular polarizations are achieved at positions that are very close to each other. We note that the peculiar spatial polarization variation is also observed when we remove the half-wave plate with a rectangular aperture; therefore, the result is not due to the Fraunhofer diffraction.

The observed phenomena are intrinsic to the reflection by the OPM. To show this, we confirmed our experimental observations by the numerical calculations as performed in Ref. 27. The E-field vector distribution is calculated by the Stratton–Chu integral equation.³¹ The integrand contains the surface current, and it is approximated by the physical optics method.³² Considering that the half-wave plate has a rectangular aperture, the OPM is supposed to be a rectangle with a side of 20 mm. The focus and the focal plane are geometrically defined.²⁷ The incident terahertz wave of 0.75 THz is linearly polarized along the Y -axis and propagates along the $-Z$ -direction. We assumed the beam profile to be Gaussian with a full-width at a half maximum of 26.6 mm to reproduce the size of the observed beam profile in Fig. 3(a).

Figures 4(a)–4(c) show the spatial distributions of $E_{Y'}(x', y', t_1)$, $E_{X'}(x', y', t_2)$, and $E_{Y'}(x', y', t_2)$ obtained by the calculation. Again, $E_{X'}(x', y', t_1)$ is almost zero in the entire focal plane. The calculation reproduces the characteristics of $E_{Y'}(x', y', t_1)$ and $E_{X'}(x', y', t_2)$ quite well; however,

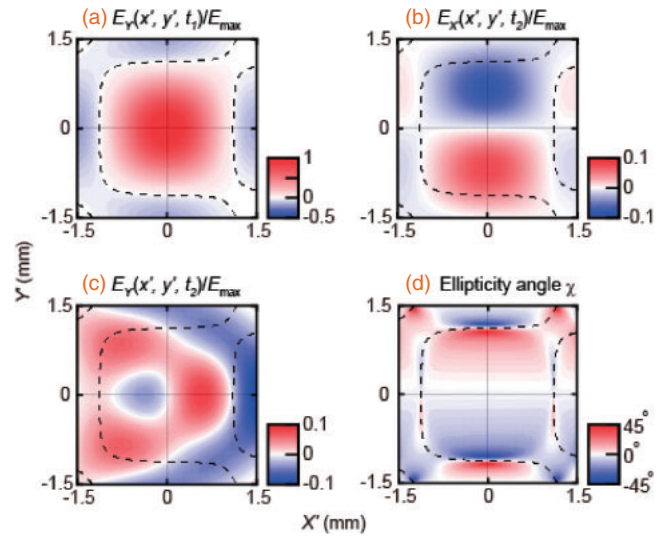


Fig. 4. Contour maps of numerical calculations of (a) $E_{Y'}(x', y', t_1)$, (b) $E_{X'}(x', y', t_2)$, (c) $E_{Y'}(x', y', t_2)$ normalized by E_{max} , and (d) ellipticity angle χ . The frequency is 0.75 THz. The dashed curve in each image represents $E_{Y'}(x', y', t_1) = 0$.

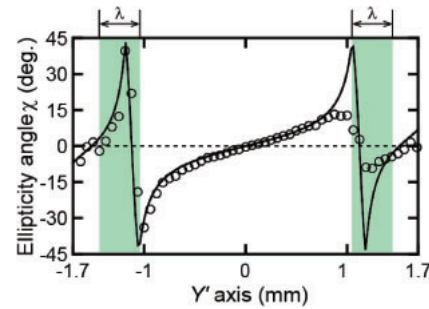


Fig. 5. Ellipticity angle χ along the Y' -axis ($x' = 0$). Circles represent the experimental result, and the curve represents a numerical calculation. The wavelength is $\lambda = 0.4 \text{ mm}$. A steep polarization change occurs around the indicated intervals.

the calculated $E_{Y'}(x', y', t_2)$ differs from the value obtained in the experiment. The discrepancy could be attributed to the imperfect alignment of the optical components in the experiment.

We would like to emphasize that the steep polarization change in the focal plane is reproduced in the calculation. Figure 4(d) shows the spatial distribution of the calculated ellipticity angle χ . Linear polarization expressed by $\chi = 0^\circ$ is realized along the X' -axis and around the curve of $E_{Y'}(x', y', t_1) = 0$. The left-handed and right-handed circular polarizations and the linear polarizations appear at very close positions.

Finally, we summarize the results obtained in the experiments and calculations. We discuss in particular the polarization property along the Y' -axis, where we observed very different behavior in the polarization state variation between the positions $|y'| \lesssim \lambda$ and $|y'| \gtrsim \lambda$, where λ (0.4 mm) is the wavelength. Figure 5 shows the spatial variation in χ along the Y' -axis. The disagreement between the experiments and calculations at $y' > 0.5 \text{ mm}$ is due to the misalignment. At the focus ($y' = 0 \text{ mm}$), the terahertz wave is linearly polarized along the Y' -axis. χ increases as $|y'|$ increases, owing to the formation of the rotational distribution at $t = t_2$ and near the focus.²⁷ For $|y'| \gtrsim \lambda$, the rotational structure collapses and a

substantial polarization change is observed. In the area, $|E_{Y'}(0, y', t_1)|$ decreases rapidly compared to $|E_{X'}(0, y', t_2)|$. Therefore, at $|y'| \approx 1.05$ mm, $|E_{Y'}(0, y', t_1)| = |E_{X'}(0, y', t_2)|$ holds, and the terahertz E-field is circularly polarized. At $|y'| \approx 1.12$ mm, $E_{Y'}(0, y', t_1)$ eventually becomes zero, and the wave is linearly polarized and the ellipticity angle becomes zero. Then, at $|y'| \approx 1.18$ mm, $|E_{Y'}(0, y', t_1)| = |E_{X'}(0, y', t_2)|$ again holds, and the wave is circularly polarized but with a different sense of rotation compared to that at the adjacent positions ($x' = 0$ mm and $y' = \pm 1.05$ mm). Finally, at $|y'| \approx 1.52$ mm, $E_{X'}(0, y', t_2)$ becomes zero, and the wave is linearly polarized along the Y' -axis. Note that these substantial polarization changes are observed within 0.47 mm on the Y' -axis, which is approximately a wavelength.

We also investigated the spatiotemporal E-field vector in the focal plane when the terahertz wave linearly polarized along the X -axis was focused by the OPM. Similar steep spatial changes in the polarization state were observed.

The results stem from the spatiotemporal distribution of the E-field vector in the focal plane. As we reported,²⁷⁾ the distribution is intrinsic to the OPM and is independent of the wavelength. The OPM used in the experiments is not symmetric about the YZ plane, whereas it is symmetric about the XZ plane. This asymmetry is an important factor of the steep polarization variation in Fig. 3. We confirmed it by performing a numerical calculation for an on-axis parabolic mirror; the calculation did not show the variation.

Finally, we emphasize that our findings are not limited to the terahertz frequency range. In short, the result is reproduced as far as the reflection by the OPM is possible; for example, we numerically confirmed it for several wavelengths in the infrared and visible frequency ranges.

In conclusion, we observed various polarization states of the terahertz wave focused by the OPM in the focal plane. In particular, we observed an abrupt change in the polarization states along the axis perpendicular to the symmetric axis of the OPM; this phenomenon is inherent to the reflection by the OPM. The amplitude of the terahertz wave that has such peculiar polarization properties is approximately one tenth of that at the focus, and it is not negligible. We confirmed the experimental results by numerical calculations. The OPMs are routinely used in THz-TDS and terahertz nonlinear optics experiments, and our findings provide useful information on these. For example, to perform the polarization-resolved terahertz time-domain spectroscopy experiments, it is important to set the sample exactly at the focus to prevent polarization state changes caused by the OPM. Another interesting example is the spin-state manipulation with different polarization states of the incident terahertz pulse within a scale of the wavelength. Thus, a precise knowledge of the polarization states in the focal plane provides many interesting possibilities for future polarization-resolved experiments.

Acknowledgments M.T. and S.W. would like to thank Dr. M. Okano for critical reading of the manuscript. This work was partially supported by the Japan Science and Technology Agency (JST) under Collaborative Research Based on

Industrial Demand “Terahertz-wave: Towards Innovative Development of Terahertz-wave Technologies and Applications”.

- 1) I. Katayama, H. Aoki, J. Takeda, H. Shimosato, M. Ashida, R. Kinjo, I. Kawayama, M. Tonouchi, M. Nagai, and K. Tanaka, *Phys. Rev. Lett.* **108**, 097401 (2012).
- 2) T. Miyamoto, H. Yada, H. Yamakawa, and H. Okamoto, *Nat. Commun.* **4**, 2586 (2013).
- 3) M. C. Hoffmann, J. Hebling, H. Y. Hwang, K.-L. Yeh, and K. A. Nelson, *Phys. Rev. B* **79**, 161201 (2009).
- 4) W. Kuehn, P. Gaal, K. Reimann, M. Woerner, T. Elsaesser, and R. Hey, *Phys. Rev. B* **82**, 075204 (2010).
- 5) M. Wagner, H. Schneider, D. Stehr, S. Winnerl, A. M. Andrews, S. Scharfner, G. Strasser, and M. Helm, *Phys. Rev. Lett.* **105**, 167401 (2010).
- 6) S. Watanabe, N. Minami, and R. Shimano, *Opt. Express* **19**, 1528 (2011).
- 7) H. Hirori, K. Shinokita, M. Shirai, S. Tani, Y. Kadoya, and K. Tanaka, *Nat. Commun.* **2**, 594 (2011).
- 8) B. Ewers, N. S. Köster, R. Woscholski, M. Koch, S. Chatterjee, G. Khitrova, H. M. Gibbs, A. C. Klettke, M. Kira, and S. W. Koch, *Phys. Rev. B* **85**, 075307 (2012).
- 9) K. Shinokita, H. Hirori, K. Tanaka, T. Mochizuki, C. Kim, H. Akiyama, L. N. Pfeiffer, and K. W. West, *Phys. Rev. Lett.* **111**, 067401 (2013).
- 10) O. Schubert, M. Hohenleutner, F. Langer, B. Urbanek, C. Lange, U. Huttner, D. Golde, T. Meier, M. Kira, S. W. Koch, and R. Huber, *Nat. Photonics* **8**, 119 (2014).
- 11) K. Yoshioka, Y. Minami, K. Shudo, T. D. Dao, T. Nagao, M. Kitajima, J. Takeda, and I. Katayama, *Nano Lett.* **15**, 1036 (2015).
- 12) R. Matsunaga, N. Tsuji, H. Fujita, A. Sugioka, K. Makise, Y. Uzawa, H. Terai, Z. Wang, H. Aoki, and R. Shimano, *Science* **345**, 1145 (2014).
- 13) K. Yamaguchi, M. Nakajima, and T. Suemoto, *Phys. Rev. Lett.* **105**, 237201 (2010).
- 14) T. Kampfrath, A. Sell, G. Klatt, A. Pashkin, S. Mahrlein, T. Dekorsy, M. Wolf, M. Fiebig, A. Leitenstorfer, and R. Huber, *Nat. Photonics* **5**, 31 (2011).
- 15) R. Zhou, Z. Jin, G. Li, G. Ma, Z. Cheng, and X. Wang, *Appl. Phys. Lett.* **100**, 061102 (2012).
- 16) Z. Jin, Z. Mics, G. Ma, Z. Cheng, M. Bonn, and D. Turchinovich, *Phys. Rev. B* **87**, 094422 (2013).
- 17) A. Pashkin, A. Sell, T. Kampfrath, and R. Huber, *New J. Phys.* **15**, 065003 (2013).
- 18) T. Kubacka, J. A. Johnson, M. C. Hoffmann, C. Vicario, S. de Jong, P. Beaud, S. Grubel, S. W. Huang, L. Huber, L. Patthey, Y. D. Chuang, J. J. Turner, G. L. Dakovski, W. S. Lee, M. P. Miniti, W. Schlotter, R. G. Moore, C. P. Hauri, S. M. Koochpayeh, V. Scagnoli, G. Ingold, S. L. Johnson, and U. Staub, *Science* **343**, 1333 (2014).
- 19) T. Nagashima and M. Hangyo, *Appl. Phys. Lett.* **79**, 3917 (2001).
- 20) R. Shimano, Y. Ino, P. S. Yu, and M. Kuwata-Gonokami, *Appl. Phys. Lett.* **81**, 199 (2002).
- 21) D. J. Aschaffenburg, M. R. C. Williams, D. Talbayev, D. F. Santavicca, D. E. Prober, and C. A. Schmuttenmaer, *Appl. Phys. Lett.* **100**, 241114 (2012).
- 22) C. M. Morris, R. V. Aguilar, A. V. Stier, and N. P. Armitage, *Opt. Express* **20**, 12303 (2012).
- 23) N. C. J. van der Valk, W. A. M. van der Marel, and P. C. M. Planken, *Opt. Lett.* **30**, 2802 (2005).
- 24) R. Zhang, Y. Cui, W. F. Sun, and Y. Zhang, *Appl. Opt.* **47**, 6422 (2008).
- 25) N. Yasumatsu and S. Watanabe, *Opt. Lett.* **37**, 2706 (2012).
- 26) H. Hirori, A. Doi, F. Blanchard, and K. Tanaka, *Appl. Phys. Lett.* **98**, 091106 (2011).
- 27) K. Shibata, M. Takai, M. Uemoto, and S. Watanabe, *Phys. Rev. A* **92**, 053806 (2015).
- 28) J. Hebling, G. Almasi, I. Kozma, and J. Kuhl, *Opt. Express* **10**, 1161 (2002).
- 29) N. Yasumatsu and S. Watanabe, *Rev. Sci. Instrum.* **83**, 023104 (2012).
- 30) M. Takai, M. Takeda, M. Sasaki, T. Tachizaki, N. Yasumatsu, and S. Watanabe, *Appl. Phys. Lett.* **105**, 151103 (2014).
- 31) J. A. Stratton and L. J. Chu, *Phys. Rev.* **56**, 99 (1939).
- 32) J. S. Asvestas, *J. Math. Phys.* **21**, 290 (1980).